

Heisenberg-scaling characterization of an arbitrary two-channel network via two-port homodyne detection

Atmadev Rai,^{1,2} Paolo Facchi,^{3,4} and Vincenzo Tamma^{1,2,5,*}

¹*School of Mathematics and Physics, University of Portsmouth, Portsmouth PO1 3QL, United Kingdom*

²*Quantum Science and Technology Hub, University of Portsmouth, Portsmouth PO1 3QL, United Kingdom*

³*Dipartimento di Fisica, Università di Bari & Politecnico di Bari, I-70126 Bari, Italy*

⁴*INFN, Sezione di Bari, I-70126 Bari, Italy*

⁵*Institute of Cosmology and Gravitation, University of Portsmouth, Portsmouth PO1 3FX, United Kingdom*

We present a fully Gaussian and experimentally feasible scheme for the simultaneous estimation of the four real parameters that characterize an arbitrary two-channel unitary transformation. The scheme utilizes a two-mode squeezed probe and balanced homodyne detection at both output ports, for which we derive the complete classical Fisher-information matrix analytically. Our scheme achieves the Heisenberg-scaling sensitivity for all four parameters simultaneously, enabling full multiparameter characterization of the generic two-channel interferometric device. We further show, by maximum-likelihood estimation, that the corresponding multiparameter Cramér-Rao bounds are saturated with a modest number of experimental repetitions and for low photon number. The scheme establishes a practical route to Heisenberg-scaling multiparameter Gaussian metrology for arbitrary two-channel networks, with direct relevance to calibration and sensing in integrated photonics and distributed quantum-enhanced measurement architectures.

Extracting multiple unknown physical quantities from the same experiment is rapidly becoming a cornerstone requirement for quantum sensing. Many realistic sensing tasks are inherently multiparametric, including quantum imaging and phase-based schemes, which require the simultaneous estimation of multiple phases [1–3], distributed sensing protocols that infer multiple phases or field components across spatially separated sensor networks [4–6], and quantum process tomography used for device characterization [7, 8]. These examples highlight the need for a multiparameter framework for quantum metrology [9, 10]. In the single-parameter setting, quantum-enhanced metrology often surpasses the classical shot-noise limit by exploiting nonclassical resources such as squeezing and entanglement, and can in principle achieve the so-called Heisenberg-limit sensitivity [11–20].

Extending single-parameter protocols to the multiparameter setting is, however, not straightforward. In general, multiparameter estimation is constrained by trade-offs due to probe and measurement incompatibility, so that simultaneously attaining the individual ultimate bound for every parameter is often not possible [10, 21]. A more practical objective is therefore to identify scalable probe states and feasible measurements that nevertheless deliver Heisenberg precision scaling as $1/N$ (with N denoting the mean photon number) simultaneously across the entire parameter space of a multiparameter estimation problem [22, 23].

Continuous-variable quantum optics provides a natural framework for this task, and Gaussian states are especially well suited because they provide both experimental robustness and a compact theoretical description [24–26]. Their statistics are fully characterized by first and second moments of the field quadratures, covering coherent

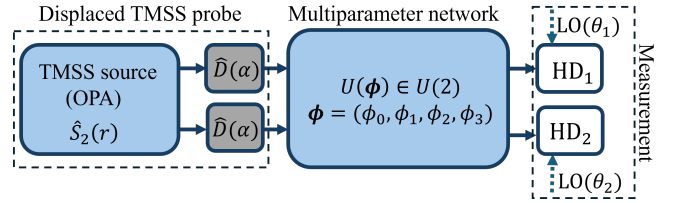


FIG. 1. A two-mode squeezed state (TMSS) (generated, for example, by an optical parametric amplifier (OPA)) probes an unknown two-channel linear-optical network described by an arbitrary unitary $U(\phi)$ in Eq. (2), with parameter vector $\phi = (\phi_0, \phi_1, \phi_2, \phi_3)$, where ϕ_3 sets the mode mixing while ϕ_1, ϕ_2 and ϕ_0 represent internal and overall phase parameters (the latter becomes operationally identifiable in the presence of a phase reference such as a local oscillator (LO)). The two output modes are measured via balanced homodyne detection (HD) at both ports, using tunable LO phases θ_1 and θ_2 .

and thermal states as well as squeezed and entangled resources. The Gaussian framework also supports robust estimation methods that perform well under finite sampling and experimental noise, which is essential when the aim is not only asymptotic scaling but also experimental feasibility.

In a two-channel setting, the most general passive linear-optical device is described by a $U(2)$ transformation, which is fully specified by four real parameters and spans the complete family of two-mode operations, including phase shifters and mode-mixing angles [27, 28]. Establishing quantum-enhanced, multiparameter estimation strategies in this setting is therefore directly relevant to precision sensing and to full characterization of photonic devices.

In this letter, we present an experimentally feasible scheme for simultaneously estimating the four real parameters of an arbitrary two-channel linear-optical net-

* vincenzo.tamma@port.ac.uk

work. Within the Gaussian framework, we consider an experimentally accessible two-mode squeezed state (TMSS) with equal displacement amplitudes injected into each input channel and perform a two-port balanced homodyne detection at the output channels of the linear network. In the scheme, we experimentally tune the local oscillator phases of the homodyne detection near the quadratures with the minimum variance using the coarse measurement outcomes. The scheme achieves Heisenberg scaling for all three phase parameters across their full domain, while the mode-mixing angle attains the Heisenberg scaling only near the balanced working point $\pi/4$. We derive the full Fisher-information matrix (FIM) and evaluate the analytical forms of the corresponding Cramér-Rao bounds (CRBs) for the four-parameter estimation problem simultaneously. Furthermore, we identify how the allocation of resources between displacement and squeezing shapes the attainable sensitivities. Our scheme is optimal in achieving the Heisenberg scaling for all parameters in the generic two-channel unitary allowed by the quantum CRB described in [29].

Quantum sensing scheme for an arbitrary unknown linear network. We describe here the quantum sensing scheme in Fig. 1 for an arbitrary, lossless two-channel linear-optical network acting on two spatial modes with annihilation operators \hat{a}_1 and \hat{a}_2 . These obey the canonical bosonic commutation relations $[\hat{a}_j, \hat{a}_k^\dagger] = \delta_{jk}$. In the absence of loss and gain, the evolution is passive and preserves the total photon number, and is therefore fully described by a unitary matrix $U \in \text{U}(2)$ that acts on the mode operators as

$$\begin{pmatrix} \hat{a}_{1,\text{out}} \\ \hat{a}_{2,\text{out}} \end{pmatrix} = U \begin{pmatrix} \hat{a}_{1,\text{in}} \\ \hat{a}_{2,\text{in}} \end{pmatrix}. \quad (1)$$

We employ the convenient parameterization

$$U = e^{-i\phi_0} \begin{pmatrix} e^{i\frac{\phi_\tau}{2}} \cos(\phi_3) & e^{i\frac{\phi_\rho}{2}} \sin(\phi_3) \\ -e^{-i\frac{\phi_\rho}{2}} \sin(\phi_3) & e^{-i\frac{\phi_\tau}{2}} \cos(\phi_3) \end{pmatrix}, \quad (2)$$

where $\phi_\tau = (\phi_1 + \phi_2)/2$ and $\phi_\rho = (\phi_1 - \phi_2)/2$ denote the phase associated with transmitted and reflected amplitudes, respectively. The mode-mixing angle $\phi_3 \in [0, \pi/2]$ fixes the transmittance and reflectance, $\tau = \cos^2(\phi_3)$ and $\rho = \sin^2(\phi_3)$, respectively, satisfying $\tau + \rho = 1$ for a lossless device. The prefactor $e^{-i\phi_0}$ fixes the global phase (and thus $\det(U) = e^{-2i\phi_0}$), while (ϕ_1, ϕ_2, ϕ_3) span an arbitrary $SU(2)$ transformation, corresponding to internal phase shifts $\phi_1, \phi_2 \in [0, 2\pi]$.

To probe the arbitrary two-channel unitary, we employ a displaced two-mode squeezed Gaussian probe,

$$|\psi_{\text{in}}\rangle = \hat{D}_1(\alpha_1) \hat{D}_2(\alpha_2) \hat{S}_{12}(\xi) |0, 0\rangle, \quad (3)$$

where $\hat{D}_j(\alpha_j) = \exp(\alpha_j \hat{a}_j^\dagger - \alpha_j^* \hat{a}_j)$ and $\hat{S}_{12}(\xi) = \exp(\xi \hat{a}_1 \hat{a}_2 - \xi^* \hat{a}_1^\dagger \hat{a}_2^\dagger)$.

For simplicity, and because it optimises the quantum Fisher information, we choose equal real displacements,

$\alpha_1 = \alpha_2 = \alpha \in \mathbb{R}$, and real squeezing, $\xi = r > 0$ [29]. We quantify the resources in terms of the mean photon numbers carried by squeezing and displacement. The average number of photons in the squeezing is $N_s = 2 \sinh^2(r)$, while the total number of displacement photons at the input is $N_c = 2\alpha^2$. The total mean photon number injected into the network is then $N = N_s + N_c$.

The output modes are then measured by balanced homodyne detection at both ports, with tunable LO phases θ_1 and θ_2 , producing joint Gaussian statistics from which all four parameters are inferred. Note that ϕ_0 multiplies the transformation as a global factor $e^{-i\phi_0(\hat{a}_1^\dagger \hat{a}_1 + \hat{a}_2^\dagger \hat{a}_2)}$ and is therefore unobservable for number-diagonal probes and POVMs. It becomes operationally identifiable once a phase reference is present. In our scheme, the homodyne detection introduces number coherence relative to the LO, so ϕ_0 rotates the output quadratures with respect to the LO and can be estimated [30].

Two-port homodyne detection and Fisher information matrix. Because both the probe state and the measurement are Gaussian, each experimental run yields a pair of real homodyne outcomes $\mathbf{x} = (x_1, x_2)^\top$ distributed according to a bivariate Gaussian distribution with mean vector $\boldsymbol{\mu}_\phi$ and covariance matrix Σ_ϕ ,

$$p(\mathbf{x} | \phi) = \frac{1}{2\pi \sqrt{\det \Sigma_\phi}} \exp \left[-\frac{1}{2} (\mathbf{x} - \boldsymbol{\mu}_\phi)^\top \Sigma_\phi^{-1} (\mathbf{x} - \boldsymbol{\mu}_\phi) \right], \quad (4)$$

where $\phi = (\phi_0, \phi_1, \phi_2, \phi_3)$ denotes the set of unknown parameters defining the two-channel network. The explicit expressions for $\boldsymbol{\mu}_\phi$ and Σ_ϕ are given in the Supplemental Material (SM) [31].

Since all four unknown parameters are encoded simultaneously in the output statistics, the analysis of the precision for the scheme requires a multiparameter estimation framework. In this setting, the attainable precision is governed by the FIM, which quantifies the local sensitivity of the likelihood $p(\mathbf{x} | \phi)$ to change in each component of ϕ and, through the multiparameter CRB, sets the best achievable covariance of any unbiased joint estimator.

For the Gaussian distributions of the form in Eq. (4), the classical FIM takes the standard form [32]

$$F_{ij} = \frac{1}{2} \text{Tr} \left[\Sigma_\phi^{-1} (\partial_i \Sigma_\phi) \Sigma_\phi^{-1} (\partial_j \Sigma_\phi) \right] + (\partial_i \boldsymbol{\mu}_\phi)^\top \Sigma_\phi^{-1} (\partial_j \boldsymbol{\mu}_\phi), \quad (5)$$

where $\partial_i \equiv \partial/\partial\phi_i$. It is convenient to write the two terms in the FIM as

$$F = F^\Sigma + F^\mu. \quad (6)$$

Here, the term F^Σ quantifies the information carried by parameter-dependent fluctuations and thus by squeezing-induced noise, whereas the term F^μ arises from the variation of parameter dependence of the mean vector $\boldsymbol{\mu}_\phi$ and is therefore associated with the homodyne signal.

Multiparameter Heisenberg scaling. We now identify the operating conditions under which the simultaneous

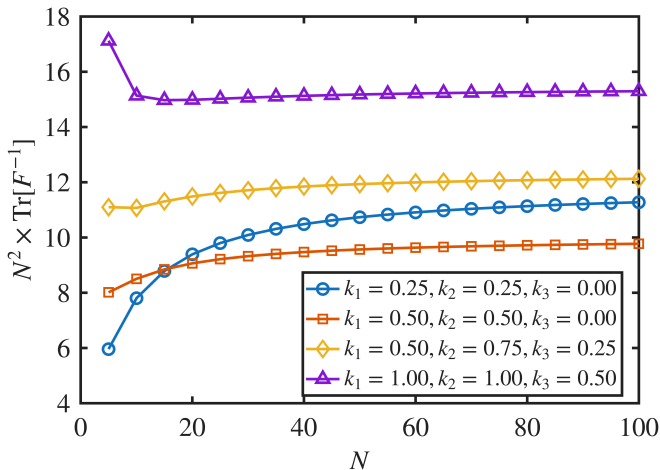


FIG. 2. The plot shows the Heisenberg-normalized scalar bound $N^2 \text{Tr}[F^{-1}]$ as a function of the total mean photon number N for several choices of k_1, k_2, k_3 . Since asymptotically $\text{Tr}[F^{-1}] \propto 1/N^2$, the curves approach an N -independent plateau, which gives the leading prefactor set by the dominant N^2 contribution \mathcal{F} to the Fisher information matrix in Eq. (10). Varying k_1, k_2, k_3 therefore changes the prefactor while preserving the $1/N^2$ scaling. Here $\beta = 1/2$.

estimation of $\phi = (\phi_0, \phi_1, \phi_2, \phi_3)$ exhibits Heisenberg scaling. To this end, we analyze the two terms of the FIM in Eq. (6). The explicit forms of Σ_ϕ and μ_ϕ reveal an important structural feature of the estimation problem: the covariance matrix Σ_ϕ is independent of the phase ϕ_1 , whereas the mean vector μ_ϕ depends on all four parameters. The independence of Σ_ϕ from ϕ_1 follows from the structure of the TMSS probe, as the relative-number fluctuation associated with ϕ_1 vanishes, i.e. $\text{Var}(\hat{N}_1 - \hat{N}_2) = 0$, where $\hat{N}_1 - \hat{N}_2$ denotes the photon-number difference operator between the channels 1 and 2, associated with the phase difference ϕ_1 . Consequently, the parameter ϕ_1 cannot be inferred from the noise term F^Σ , its Fisher information enters only through F^μ , via the displacement-induced response of the homodyne signal. By contrast, ϕ_0, ϕ_2 , and ϕ_3 are encoded in both the mean vector and the covariance matrix [31].

To make the Heisenberg scaling explicit in an experimentally controlled way, the LO phases can be tuned so that each detector measures close to the minimum-variance quadratures of the corresponding output modes. Specifically, the LO phases follow the asymptotic form

$$\theta_i = f_i + \frac{k_i}{N_s}, \quad i = 1, 2, \quad (7)$$

where f_i denotes the phase of the quadrature fields \hat{x}_{i,f_i} at which the variance of output mode i is minimized. In other words, the LO phases are detuned from the minimum f_i by an additional term k_i/N_s where k_i is an arbitrary constant independent of N . For our parameterization, $f_1 = \phi_0 + \phi_2/2$ and $f_2 = \pi/2 + \phi_0 - \phi_2/2$, which can be obtained experimentally by minimizing Σ_ϕ from a coarse estimation of the output second moments. We

furthermore operate the mode mixing parameter close to the balanced working point, $\phi_3 = \pi/4 + \delta\phi_3$, this is an experimentally relevant situation in which the beam splitter is tuned near a balanced mixing angle, while allowing small deviations. In the asymptotic analysis we take $\delta\phi_3 = k_3/N_s$ with k_3 independent of N .

A detailed derivation of the FIM is given in Sec. II of the SM [31]. Under the LO-tuning condition (7) and operating the beam splitter near the balanced point in ϕ_3 , we substitute the derivatives of Σ_ϕ and μ_ϕ into Eq. (5) and expand for large photon number N with $N_{s,c} = O(N)$. The two contributions to the FIM then take the asymptotic forms

$$F^\Sigma = N_s^2 \mathcal{F}^\Sigma(k_1, k_2, k_3) + O(N), \quad (8)$$

$$F^\mu = N_s N_c \mathcal{F}^\mu(k_1, k_2, k_3) + O(N). \quad (9)$$

Here \mathcal{F}^Σ and \mathcal{F}^μ are 4×4 coefficient matrices independent of N and are given in [31]. The term F^Σ , which arises from the fluctuation of homodyne outcomes, depends solely on squeezing in the probe and scales as N_s^2 . It therefore gives the leading N^2 information for the parameters encoded in the covariance, namely ϕ_0, ϕ_2 , and ϕ_3 . Whereas, ϕ_1 rotates only the measured quadrature signal in phase space and thus enters only through the homodyne mean μ_ϕ . Since Σ_ϕ is independent of ϕ_1 , its Fisher information contribution is carried only by F^μ , with leading scaling $N_s N_c$. The coherent displacement is therefore essential for rendering the full four-parameter problem identifiable at Heisenberg scaling.

With the resource scaling $N_s = \beta N$ and $N_c = (1-\beta)N$, where $\beta \in (0, 1)$, the total FIM can be asymptotically written by combining the two contributions as

$$F = N^2 \mathcal{F}(k_1, k_2, k_3, \beta) + O(N), \quad (10)$$

where $\mathcal{F} = \beta^2 \mathcal{F}^\Sigma + \beta(1-\beta) \mathcal{F}^\mu$. The $O(N^2)$ term of the Fisher matrix is sufficient to establish Heisenberg-scaling behavior of the parameter sensitivities for the non-singular coefficient matrix \mathcal{F} . For the multiparameter analysis, the results of the calculation for F^{-1} are shown in Fig. 2, which shows that the N^2 -rescaled scalar quantity $N^2 \text{Tr}[F^{-1}]$ approaches an N -independent plateau, confirming the asymptotic Heisenberg scaling $\text{Tr}[F^{-1}] \propto 1/N^2$. In particular, for any (locally) unbiased estimator $\tilde{\phi} = (\tilde{\phi}_0, \tilde{\phi}_1, \tilde{\phi}_2, \tilde{\phi}_3)$ of ϕ and for M independent experimental repetitions, the marginal estimator variance denoted by $\text{Var}(\tilde{\phi}) \equiv \Delta^2 \tilde{\phi}$ asymptotically read [33]

$$\Delta^2 \tilde{\phi}_0 \geq (\Delta^2 \phi_0)^{\text{CRB}} = \frac{1}{M N^2} [\mathcal{F}^{-1}]_{11}, \quad (11)$$

$$\Delta^2 \tilde{\phi}_1 \geq (\Delta^2 \phi_1)^{\text{CRB}} = \frac{1}{M N^2} [\mathcal{F}^{-1}]_{22}, \quad (12)$$

$$\Delta^2 \tilde{\phi}_2 \geq (\Delta^2 \phi_2)^{\text{CRB}} = \frac{1}{M N^2} [\mathcal{F}^{-1}]_{33}, \quad (13)$$

$$\Delta^2 \tilde{\phi}_3 \geq (\Delta^2 \phi_3)^{\text{CRB}} = \frac{1}{M N^2} [\mathcal{F}^{-1}]_{44}. \quad (14)$$

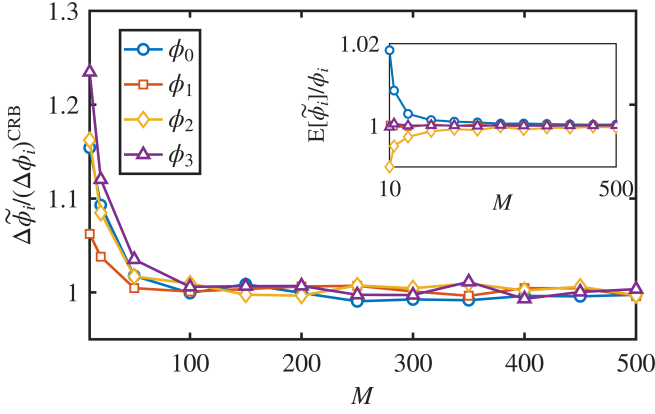


FIG. 3. Maximum likelihood estimation of the four parameters under the two-port homodyne detection for $N = 10$ and $\beta = 1/2$. The main panel shows the normalized CRB $\Delta\tilde{\phi}_i/(\Delta\phi_i)^{\text{CRB}}$ with $i = 0, 1, 2, 3$ as a function of the number of measurement repetitions M , where $\Delta\tilde{\phi}_i$ is the standard deviation of the estimator and $(\Delta\phi_i)^{\text{CRB}}$ is the corresponding marginal CRB in Eqs. (11)–(14). The convergence of all four curves to unity confirms the saturation of the CRBs already for a relatively small number M of experimental iterations, typically $M \approx 100$. In the inset, we plot the ratio between the expected value $E[\tilde{\phi}_i]$ of the maximum-likelihood estimator and the true value ϕ_i . Here, $k_1 = k_2 = 0.5$ and $k_3 = 0$.

These bounds demonstrate simultaneous Heisenberg-scaling estimation for all four parameters, provided the k_i values are chosen such that the leading-order coefficient matrix \mathcal{F} is nonsingular [31]. For example, for $\beta = 1/2$, $k_1 = k_2 = 1/2$, and $k_3 = 0$, one finds $\text{diag}(\mathcal{F}^{-1}) = (1, 4, 4, 1)$, so the corresponding CRBs therefore scale as $\Delta^2\tilde{\phi}_0 \geq 1/(MN^2)$, $\Delta^2\tilde{\phi}_1 \geq 4/(MN^2)$, $\Delta^2\tilde{\phi}_2 \geq 4/(MN^2)$, and $\Delta^2\tilde{\phi}_3 \geq 1/(MN^2)$ at leading order. The balanced resource split $\beta = 1/2$ (i.e., $N_s = N_c$) maximizes the leading contribution F^μ in Eq. (9), since it scales as $N_s N_c$. By contrast, minimizing the scalar bound (sum of the CRBs) $\text{Tr}[F^{-1}]$ typically favors $\beta > 1/2$, since three of the four parameters derive their leading information from the squeezing-dominated contribution $F^\Sigma \propto N_s^2$. For simplicity, we choose $\beta = 1/2$ throughout the text.

Further, we go beyond stating the bounds and demonstrate the attainability of the CRBs by applying maximum-likelihood estimation (MLE). We implement the MLE for all four parameters and show that it asymptotically saturates the CRBs in Eqs. (11)–(14), thus achieving Heisenberg-scaling precision. The derivation of the maximum-likelihood estimator for this scheme is given in SM [31]. Figures 3 and 4 illustrate its behavior, confirming the saturation of the CRB for all parameters simultaneously already for a sample size of the order $M \approx 100$ and for a relatively small average number of photons in the squeezed and coherent states. The insets show the ratio of the expected value $E[\tilde{\phi}_i]$ of the estimator and the true value ϕ_i approaching unity, confirming that

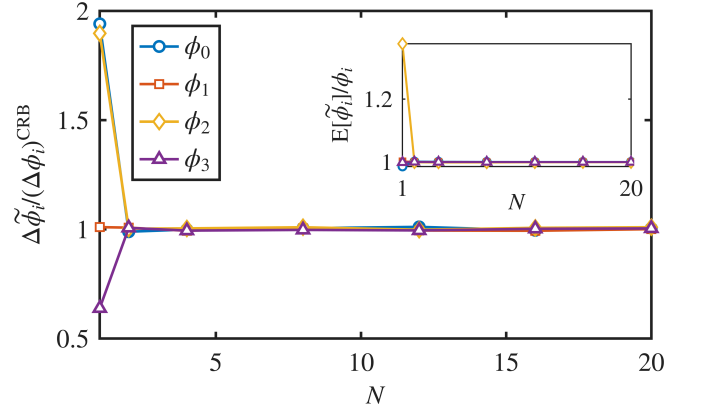


FIG. 4. Maximum likelihood estimation of ϕ as a function of the total mean photon number N at a fixed sample size $M = 200$. The main panel shows convergence of the normalized CRB $\Delta\tilde{\phi}_i/(\Delta\phi_i)^{\text{CRB}}$ for each parameter in Eqs. (11)–(14) saturating the CRBs already at low photon numbers. The inset shows the unbiasedness ratio $E[\tilde{\phi}_i]/\phi_i$, confirming the estimator remains effectively unbiased for small values of N . Here, $k_1 = k_2 = 0.5$, $k_3 = 0$ and $\beta = 1/2$ for all N .

the estimator bias vanishes for the same order of sample size M and the total mean photon number N . These results provide direct numerical validation that the multiparameter MLEs saturate the CRBs and achieve the Heisenberg-scaling precision. Our scheme remains robust for the different parameter values ϕ_0 , ϕ_1 , and ϕ_2 (see Fig. S2 in SM [31]), as far as ϕ_3 is operated close to $\pi/4$.

Conclusions. We have introduced a fully Gaussian and experimentally realistic scheme for the simultaneous estimation of the full set of four real parameters defining an arbitrary two-channel linear-optical transformation $U(2)$ using a displaced two-mode squeezed probe and two-port balanced homodyne detection. Working within the classical estimation framework defined by the homodyne statistics, we derive the FIM and corresponding multiparameter CRBs, and we identify operating conditions under which the attainable precision exhibits Heisenberg scaling.

Our results show that three of the parameters are predominantly encoded in the squeezing controlled fluctuations, so their precision is governed by the covariance contribution F^Σ , whereas, the parameter ϕ_1 is accessed primarily through the signal of the homodyne outcome, and its Fisher information is therefore given by F^μ , highlighting the essential role of the displacement to estimate all four parameters simultaneously.

Our analysis also shows the practical conditions required to achieve the Heisenberg scaling. The mode-mixing angle ϕ_3 must be operated close to the balanced point $\pi/4$, in addition, optimal sensitivity requires tuning of the LO phases θ_1 and θ_2 using coarse prior estimates of ϕ_0 and ϕ_2 .

Finally, we demonstrate the attainability using the ex-

act Gaussian likelihood for the homodyne outcomes, we construct a maximum-likelihood estimator and show that it approaches the CRB already for modest data size, of the order of 100 experimental runs, and even at a few mean photon number. The saturation of the CRBs for fewer experimental iterations and photon numbers is essential for realistic sensing and device characterization scenarios.

ACKNOWLEDGMENTS

This work was partially supported by Xairos System Inc. VT also acknowledges partial support from the Air

Force Office of Scientific Research under award number FA8655-23-17046. PF was partially supported by Istituto Nazionale di Fisica Nucleare (INFN) through the project “QUANTUM”, by the Italian National Group of Mathematical Physics (GNFM-INdAM), and by the Italian funding within the “Budget MUR - Dipartimenti di Eccellenza 2023–2027” - Quantum Sensing and Modelling for One-Health (QuaSiModO).

-
- [1] Peter C. Humphreys, Marco Barbieri, Animesh Datta, and Ian A. Walmsley, “Quantum enhanced multiple phase estimation,” *Phys. Rev. Lett.* **111**, 070403 (2013).
- [2] Christos N. Gagatsos, Dominic Branford, and Animesh Datta, “Gaussian systems for quantum-enhanced multiple phase estimation,” *Phys. Rev. A* **94**, 042342 (2016).
- [3] Francesco Albarelli, Marco Barbieri, Marco G Genoni, and Ilaria Gianani, “A perspective on multiparameter quantum metrology: From theoretical tools to applications in quantum imaging,” *Physics Letters A* **384**, 126311 (2020).
- [4] Quntao Zhuang, Zheshen Zhang, and Jeffrey H. Shapiro, “Distributed quantum sensing using continuous-variable multipartite entanglement,” *Phys. Rev. A* **97**, 032329 (2018).
- [5] Timothy J. Proctor, Paul A. Knott, and Jacob A. Dunningham, “Multiparameter estimation in networked quantum sensors,” *Phys. Rev. Lett.* **120**, 080501 (2018).
- [6] Xueshi Guo, Casper R Breum, Johannes Borregaard, Shuro Izumi, Mikkel V Larsen, Tobias Gehring, Matthias Christandl, Jonas S Neergaard-Nielsen, and Ulrik L Andersen, “Distributed quantum sensing in a continuous-variable entangled network,” *Nature Physics* **16**, 281–284 (2020).
- [7] Xiao-Qi Zhou, Hugo Cable, Rebecca Whittaker, Peter Shadbolt, Jeremy L O’Brien, and Jonathan CF Matthews, “Quantum-enhanced tomography of unitary processes,” *Optica* **2**, 510–516 (2015).
- [8] Yonatan Gazit, Hui Khoon Ng, and Jun Suzuki, “Quantum process tomography via optimal design of experiments,” *Phys. Rev. A* **100**, 012350 (2019).
- [9] Magdalena Szczykulska, Tillmann Baumgratz, and Animesh Datta, “Multi-parameter quantum metrology,” *Advances in Physics: X* **1**, 621–639 (2016).
- [10] F. Albarelli, M. Barbieri, M.G. Genoni, and I. Gianani, “A perspective on multiparameter quantum metrology: From theoretical tools to applications in quantum imaging,” *Physics Letters A* **384**, 126311 (2020).
- [11] Carlton M. Caves, “Quantum-mechanical noise in an interferometer,” *Phys. Rev. D* **23**, 1693–1708 (1981).
- [12] M. J. Holland and K. Burnett, “Interferometric detection of optical phase shifts at the heisenberg limit,” *Phys. Rev. Lett.* **71**, 1355–1358 (1993).
- [13] Roy S. Bondurant and Jeffrey H. Shapiro, “Squeezed states in phase-sensing interferometers,” *Phys. Rev. D* **30**, 2548–2556 (1984).
- [14] Vittorio Giovannetti, Seth Lloyd, and Lorenzo Maccone, “Quantum metrology,” *Phys. Rev. Lett.* **96**, 010401 (2006).
- [15] Jonathan P Dowling and Kaushik P Seshadreesan, “Quantum optical technologies for metrology, sensing, and imaging,” *Journal of Lightwave Technology* **33**, 2359–2370 (2015).
- [16] Sisi Zhou, Mengzhen Zhang, John Preskill, and Liang Jiang, “Achieving the heisenberg limit in quantum metrology using quantum error correction,” *Nature communications* **9**, 78 (2018).
- [17] Kevin Qian, Zachary Eldredge, Wenchao Ge, Guido Pagano, Christopher Monroe, James V Porto, and Alexey V Gorshkov, “Heisenberg-scaling measurement protocol for analytic functions with quantum sensor networks,” *Physical Review A* **100**, 042304 (2019).
- [18] Vittorio Giovannetti, Seth Lloyd, and Lorenzo Maccone, “Quantum-enhanced measurements: Beating the standard quantum limit,” *Science* **306**, 1330–1336 (2004), <https://www.science.org/doi/pdf/10.1126/science.1104149>.
- [19] Luca Pezzé and Augusto Smerzi, “Entanglement, nonlinear dynamics, and the heisenberg limit,” *Phys. Rev. Lett.* **102**, 100401 (2009).
- [20] Nicolai Friis, Michalis Skotiniotis, Ivette Fuentes, and Wolfgang Dür, “Heisenberg scaling in gaussian quantum metrology,” *Phys. Rev. A* **92**, 022106 (2015).
- [21] Francesco Albarelli and Rafał Demkowicz-Dobrzański, “Probe incompatibility in multiparameter noisy quantum metrology,” *Physical Review X* **12**, 011039 (2022).
- [22] Giovanni Gramegna, Danilo Triggiani, Paolo Facchi, Frank A. Narducci, and Vincenzo Tamma, “Typicality of heisenberg scaling precision in multimode quantum metrology,” *Phys. Rev. Res.* **3**, 013152 (2021).
- [23] Atmadev Rai, Danilo Triggiani, Paolo Facchi, and Vincenzo Tamma, “Heisenberg-scaling precision in the estimation of two parameters in a mach-zehnder interferometer,” *Phys. Rev. A* **111**, 062408 (2025).
- [24] Alessandro Ferraro, Stefano Olivares, and Matteo GA Paris, “Gaussian states in continuous variable quantum information,” arXiv preprint quant-ph/0503237 (2005).

- [25] Samuel L Braunstein and Peter Van Loock, “Quantum information with continuous variables,” *Reviews of modern physics* **77**, 513–577 (2005).
- [26] Gerardo Adesso and Fabrizio Illuminati, “Entanglement in continuous-variable systems: recent advances and current perspectives,” *Journal of Physics A: Mathematical and Theoretical* **40**, 7821 (2007).
- [27] Richard A. Campos, Bahaa E. A. Saleh, and Malvin C. Teich, “Quantum-mechanical lossless beam splitter: $Su(2)$ symmetry and photon statistics,” *Phys. Rev. A* **40**, 1371–1384 (1989).
- [28] Andrés Macho-Ortiz, Daniel Pérez-López, and José Capmany, “Optical implementation of 2×2 universal unitary matrix transformations,” *Laser & Photonics Reviews* **15**, 2000473 (2021).
- [29] Atmadev Rai, Danilo Triggiani, Paolo Facchi, and Vincenzo Tamma, “Multiparameter quantum metrology at heisenberg scaling for an arbitrary two-channel linear interferometer with squeezed light,” *Phys. Rev. A* **112**, 062401 (2025).
- [30] Luca Pezzè, Philipp Hyllus, and Augusto Smerzi, “Phase-sensitivity bounds for two-mode interferometers,” *Phys. Rev. A* **91**, 032103 (2015).
- [31] See Supplemental Material at (URL will be inserted by the publisher).
- [32] Harald Cramér, *Mathematical methods of statistics*, Vol. 9 (Princeton university press, Princeton, 1999).
- [33] Carl W Helstrom, “Quantum detection and estimation theory,” *Journal of Statistical Physics* **1**, 231–252 (1969).

Supplemental Material

Heisenberg-scaling characterization of an arbitrary two-channel network via two-port homodyne detection

Atmadev Rai,^{1,2} Paolo Facchi,^{3,4} and Vincenzo Tamma^{1,2,5}

¹School of Mathematics and Physics, University of Portsmouth, Portsmouth PO1 3QL, United Kingdom

²Quantum Science and Technology Hub, University of Portsmouth, Portsmouth PO1 3QL, United Kingdom

³Dipartimento di Fisica, Università di Bari & Politecnico di Bari, I-70126 Bari, Italy

⁴INFN, Sezione di Bari, I-70126 Bari, Italy

⁵Institute of Cosmology and Gravitation, University of Portsmouth, Portsmouth PO1 3FX, United Kingdom

I. GAUSSIAN STATISTICS: TWO-PORT HOMODYNE DETECTION

In this section, we derive the Gaussian probability distribution (4) for two-port homodyne detection at the output of an arbitrary unitary $U(2)$ network probed by a TMSS,

$$|\psi_{\text{in}}\rangle = \hat{D}_1(\alpha_1) \hat{D}_2(\alpha_2) \hat{S}_{12}(\xi) |0, 0\rangle, \quad (\text{S1})$$

where $\hat{D}_i(\alpha_i)$ is the single-mode displacement operator acting on mode i with $\alpha_i = |\alpha_i|e^{i\beta_i}$ for $i = 1, 2$, and $\hat{S}_{12}(\xi)$ is the two-mode squeezing operator with complex squeezing parameter $\xi = re^{i\theta}$. For simplicity, and without loss of optimality for the quantum Fisher information matrix, we restrict to equal real displacements in both input modes, $|\alpha_1| = |\alpha_2| = |\alpha|$ and $\beta_1 = \beta_2 = 0$, and to real squeezing, $\xi = r$ with $\theta = 0$, which satisfies the optimality condition $\theta - \beta_1 - \beta_2 = 0$ [29].

Adopting the quadrature ordering $\mathbf{z} = (x_1, p_1, x_2, p_2)^\top$, the initial displacement vector of the input state (S1) is $\mathbf{d}_0 = \sqrt{2}|\alpha|(1, 0, 1, 0)^\top$, and the covariance matrix of the two-mode squeezed vacuum $\hat{S}_{12}(r)|0, 0\rangle$ is

$$\Gamma_0 = \frac{1}{2} \begin{pmatrix} \cosh(2r) & 0 & \sinh(2r) & 0 \\ 0 & \cosh(2r) & 0 & -\sinh(2r) \\ \sinh(2r) & 0 & \cosh(2r) & 0 \\ 0 & -\sinh(2r) & 0 & \cosh(2r) \end{pmatrix}. \quad (\text{S2})$$

After the action of the arbitrary two-channel network U_ϕ , the displacement and covariance matrix transform as

$$\mathbf{d}_\phi = R_\phi \mathbf{d}_0, \quad \Gamma_\phi = R_\phi \Gamma_0 R_\phi^\top, \quad (\text{S3})$$

where R_ϕ is the real orthogonal symplectic matrix associated with the unitary U_ϕ ,

$$R_\phi = \begin{pmatrix} \text{Re}[U_\phi] & -\text{Im}[U_\phi] \\ \text{Im}[U_\phi] & \text{Re}[U_\phi] \end{pmatrix}. \quad (\text{S4})$$

We then perform homodyne measurements on both output ports of the network. On mode $j = 1, 2$ we measure the quadrature $\hat{x}_{\theta_j}^{(j)} = \frac{1}{\sqrt{2}}(e^{-i\theta_j}\hat{a}_{j,\text{out}} + e^{i\theta_j}\hat{a}_{j,\text{out}}^\dagger)$, rotated by the LO phase θ_j . Collecting the two measurement outcomes into the vector $\mathbf{x} = (x_1, x_2)^\top$, where x_j is the eigenvalue of $\hat{x}_{\theta_j}^{(j)}$, the measured observables can be written as linear combinations of the output quadratures,

$$\hat{\mathbf{x}} = M \hat{\mathbf{z}}_\phi, \quad (\text{S5})$$

where $\hat{\mathbf{z}}_\phi$ is the output quadrature operator vector and the 2×4 matrix M is

$$M = \begin{pmatrix} \cos(\theta_1) & \sin(\theta_1) & 0 & 0 \\ 0 & 0 & \cos(\theta_2) & \sin(\theta_2) \end{pmatrix}. \quad (\text{S6})$$

Since the input state is Gaussian and the transformation U_ϕ is linear and passive, the joint statistics of (x_1, x_2) remain Gaussian. The corresponding mean vector and covariance matrix are $\boldsymbol{\mu}_\phi = M \mathbf{d}_\phi$ and $\Sigma_\phi = M \Gamma_\phi M^\top$, respectively. The joint probability density of observing outcomes $\mathbf{x} = (x_1, x_2)^\top$ is therefore

$$p(\mathbf{x} | \phi) = \frac{1}{2\pi\sqrt{\det \Sigma_\phi}} \exp\left[-\frac{1}{2}(\mathbf{x} - \boldsymbol{\mu}_\phi)^\top \Sigma_\phi^{-1}(\mathbf{x} - \boldsymbol{\mu}_\phi)\right], \quad (\text{S7})$$

as in Eq. (4) in the main text. For the parameter vector $\boldsymbol{\phi} = (\phi_0, \phi_1, \phi_2, \phi_3)$ of the arbitrary two-channel network $U_{\boldsymbol{\phi}}$, the mean vector and covariance matrix can be written explicitly as

$$\boldsymbol{\mu}_{\boldsymbol{\phi}} = \sqrt{2} |\alpha| \begin{pmatrix} \cos(\phi_3) \cos\left(\frac{1}{2}(2\theta_1 - \phi_1 - 2\phi_0 - \phi_2)\right) + \sin(\phi_3) \cos\left(\frac{1}{2}(2\theta_1 + \phi_1 - 2\phi_0 - \phi_2)\right) \\ \cos(\phi_3) \cos\left(\frac{1}{2}(2\theta_2 + \phi_1 - 2\phi_0 + \phi_2)\right) - \sin(\phi_3) \cos\left(\frac{1}{2}(2\theta_2 - \phi_1 - 2\phi_0 + \phi_2)\right) \end{pmatrix}, \quad (\text{S8})$$

$$\Sigma_{\boldsymbol{\phi}} = \frac{1}{2} \begin{pmatrix} \cosh(2r) - \sin(2\phi_3) \cos(2\theta_1 - 2\phi_0 - \phi_2) \sinh(2r) & -\cos(2\phi_3) \sinh(2r) \cos(\theta_1 + \theta_2 - 2\phi_0) \\ -\cos(2\phi_3) \sinh(2r) \cos(\theta_1 + \theta_2 - 2\phi_0) & \cosh(2r) + \sin(2\phi_3) \cos(2\theta_2 - 2\phi_0 + \phi_2) \sinh(2r) \end{pmatrix}. \quad (\text{S9})$$

II. DERIVATION OF THE FISHER INFORMATION MATRIX

A. Asymptotic form of F^{Σ} in Eq. (8)

We begin with the first term in Eq. (5) of the main text,

$$F_{ij}^{\Sigma} = \frac{1}{2} \text{Tr} \left[\Sigma_{\boldsymbol{\phi}}^{-1} (\partial_i \Sigma_{\boldsymbol{\phi}}) \Sigma_{\boldsymbol{\phi}}^{-1} (\partial_j \Sigma_{\boldsymbol{\phi}}) \right], \quad (\text{S10})$$

where $\Sigma_{\boldsymbol{\phi}}$ is given explicitly in Eq. (S9). Expressed in terms of the average photon number of the TMSS, $N_s = 2 \sinh^2(r)$, the covariance matrix reads

$$\Sigma_{\boldsymbol{\phi}} = \frac{1}{2} \begin{pmatrix} N_s + 1 - \sqrt{N_s(N_s + 2)} \cos(2\theta_1 - 2\phi_0 - \phi_2) \sin(2\phi_3) & -\sqrt{N_s(N_s + 2)} \cos(\theta_1 + \theta_2 - 2\phi_0) \cos(2\phi_3) \\ -\sqrt{N_s(N_s + 2)} \cos(\theta_1 + \theta_2 - 2\phi_0) \cos(2\phi_3) & N_s + 1 + \sqrt{N_s(N_s + 2)} \cos(2\theta_2 - 2\phi_0 + \phi_2) \sin(2\phi_3) \end{pmatrix}. \quad (\text{S11})$$

Since $\sqrt{N_s(N_s + 1)} = O(N_s)$ and all trigonometric factors are bounded, each entry of $\Sigma_{\boldsymbol{\phi}}$ is at most $O(N_s)$, and same holds for its parameter derivatives, i.e. $\partial_{\phi_i} \Sigma_{\boldsymbol{\phi}} = O(N_s)$. Therefore for generic LO phases, the determinant scales as $\det(\Sigma_{\boldsymbol{\phi}}) = O(N_s^2)$, while the adjoint matrix $\text{adj}(\Sigma_{\boldsymbol{\phi}})$ has entries of order $O(N_s)$. Using $\Sigma_{\boldsymbol{\phi}}^{-1} = \text{adj}(\Sigma_{\boldsymbol{\phi}})/\det(\Sigma_{\boldsymbol{\phi}})$ therefore yields $\Sigma_{\boldsymbol{\phi}}^{-1} = O(N_s^{-1})$. Consequently, the matrix product inside the trace in Eq. (S10) is $O(N_s^0)$, resulting in $F_{ij}^{\Sigma} = O(N_s^0)$.

Therefore, to achieve the Heisenberg-scaling sensitivity, we tune the homodyne phases to the minimum-variance quadratures according to condition (7) of the main text. We tune the LO phases as $\theta_1 = f_1 + k_1/N_s$ and $\theta_2 = f_2 + k_2/N_s$, where $f_1 = \phi_0 + \phi_2/2$, $f_2 = \pi/2 + \phi_0 - \phi_2/2$ are the quadrature angles that minimize the variances of modes 1 and 2, respectively. In practice, these angles can be identified from a coarse estimation of the output second moments and by locating the corresponding minima. We also operate close to a balanced beam splitter, $\phi_3 = \pi/4 + \delta\phi_3$, and in the asymptotic expansion we take $\delta\phi_3 = k_3/N_s$, where k_1, k_2, k_3 are N -independent constants. Under these conditions, the covariance matrix admits the asymptotic form

$$\Sigma_{\boldsymbol{\phi}} = \begin{pmatrix} \frac{1+4k_1^2+4k_3^2}{4N_s} + O\left(\frac{1}{N_s^2}\right) & -\frac{(k_1+k_2)k_3}{N_s} + O\left(\frac{1}{N_s^2}\right) \\ -\frac{(k_1+k_2)k_3}{N_s} + O\left(\frac{1}{N_s^2}\right) & \frac{1+4k_2^2+4k_3^2}{4N_s} + O\left(\frac{1}{N_s^2}\right) \end{pmatrix}. \quad (\text{S12})$$

Evaluating $\Sigma_{\boldsymbol{\phi}}^{-1}$ and $\partial_i \Sigma_{\boldsymbol{\phi}}$ in the same conditions and substituting into Eq. (5), the FIM F^{Σ} asymptotically reads as in Eq. (8) in the main text

$$F^{\Sigma} = N_s^2 \mathcal{F}^{\Sigma} + O(N_s), \quad (\text{S13})$$

with the coefficient matrix

$$\mathcal{F}^{\Sigma} = \frac{1}{\Lambda^2} \begin{pmatrix} D_1 & 0 & A & B \\ 0 & 0 & 0 & 0 \\ A & 0 & D_3 & C \\ B & 0 & C & D_4 \end{pmatrix}, \quad (\text{S14})$$

where $\Lambda \equiv (1 + 4k_1^2)(1 + 4k_2^2) + 8(1 - 4k_1k_2)k_3^2 + 16k_3^4$, and the nonzero matrix elements are

$$D_1 = 32 \left[k_2^2 + k_1^2 (1 + 16k_2^2(1 + k_1^2 + k_2^2)) + 2k_3^2 - 32k_1k_2(1 + k_1^2 - k_1k_2 + k_2^2)k_3^2 + 16(1 + k_1^2 - 4k_1k_2 + k_2^2)k_3^4 + 32k_3^6 \right], \quad (\text{S15})$$

$$D_3 = 8 \left[k_2^2 + k_1^2 (1 + 16k_2^2(1 + k_1^2 + k_2^2)) - 8(-1 + 4k_1k_2)(k_1^2 + k_2^2)k_3^2 + 16(k_1^2 + k_2^2)k_3^4 \right], \quad (\text{S16})$$

$$D_4 = 16 \left[(1 + 4k_1^2)(k_1 + k_2)^2(1 + 4k_2^2) - 4(-1 + 2(k_1^2 + 6k_1k_2 + 4k_1^3k_2 + k_2^2 + 4k_1k_2^3))k_3^2 + 16(2 + k_1^2 - 6k_1k_2 + k_2^2)k_3^4 + 64k_3^6 \right]. \quad (\text{S17})$$

$$A = -16(k_1^2 - k_2^2)(-1 + 4k_1k_2 - 4k_3^2)(1 + 4k_1k_2 - 4k_3^2), \quad (\text{S18})$$

$$B = 64(k_1 + k_2)k_3(-1 + 4k_1k_2 - 4k_3^2)(1 + 4k_1k_2 - 4k_3^2), \quad (\text{S19})$$

$$C = -16(k_1 - k_2)k_3(-1 - 2k_2 + k_1(-2 + 4k_2) - 4k_3^2)(-1 + 2k_2 + k_1(2 + 4k_2) - 4k_3^2). \quad (\text{S20})$$

Equations (S15)–(S20) collect all $O(N_s^2)$ coefficients, which are the only ones that contribute to Heisenberg scaling.

B. Asymptotic form of F^μ in Eq. (9)

The FIM contribution from the derivatives of the mean homodyne signal is given by

$$F_{ij}^\mu = (\partial_i \boldsymbol{\mu}_\phi)^\top \Sigma_\phi^{-1} (\partial_j \boldsymbol{\mu}_\phi), \quad (\text{S21})$$

and depends on both the coherent displacement and the squeezing through $\boldsymbol{\mu}_\phi$ and Σ_ϕ . In the same conditions (7) and for $\phi_3 = \pi/4 + k_3/N_s$ by substituting the parameter derivatives of the mean $\boldsymbol{\mu}_\phi$ (S8) and Σ_ϕ^{-1} into F^μ yields, to the leading order,

$$F^\mu = N_s N_c \mathcal{F}^\mu(k_1, k_2, k_3, \phi_1) + O(N) \quad (\text{S22})$$

where the coefficient matrix is independent of N . Explicitly,

$$\mathcal{F}^\mu = \frac{2}{\Lambda} \begin{pmatrix} 0 & 0 & 0 & 0 \\ 0 & D_2 & 0 & 0 \\ 0 & 0 & 0 & 0 \\ 0 & 0 & 0 & 0 \end{pmatrix}, \quad (\text{S23})$$

with

$$D_2 = 1 + 2k_1^2 + 2k_2^2 + 4k_3^2 + 2(k_1 + k_2)[(k_1 - k_2) \cos(\phi_1) + 2k_3 \sin(\phi_1)]. \quad (\text{S24})$$

We find that the only entry with a leading $O(N_s N_c) = O(N^2)$ contribution is the $[F^\mu]_{22}$ component, while all other entries are at most $O(N)$ or $O(N^0)$, since $N_{s,c} = O(N)$.

C. Total asymptotic FIM and CRBs

Introducing the resource split $N_s = \beta N$, $N_c = (1 - \beta)N$ for any value $0 < \beta < 1$ independent of N , and combining the two contributions of the FIM in Eq. (S13) and Eq. (S22), the total FIM up to the leading order reads,

$$F = F^\Sigma + F^\mu = N^2 \mathcal{F}(k_1, k_2, k_3, \beta) + O(N), \quad (\text{S25})$$

where the leading-order coefficient matrix $\mathcal{F} = \mathcal{F}^\Sigma + \mathcal{F}^\mu$ is

$$\mathcal{F} = \frac{\beta^2}{\Lambda^2} \begin{pmatrix} D_1 & 0 & A & B \\ 0 & 0 & 0 & 0 \\ A & 0 & D_3 & C \\ B & 0 & C & D_4 \end{pmatrix} + \frac{2(1 - \beta)\beta}{\Lambda} \begin{pmatrix} 0 & 0 & 0 & 0 \\ 0 & D_2 & 0 & 0 \\ 0 & 0 & 0 & 0 \\ 0 & 0 & 0 & 0 \end{pmatrix}. \quad (\text{S26})$$

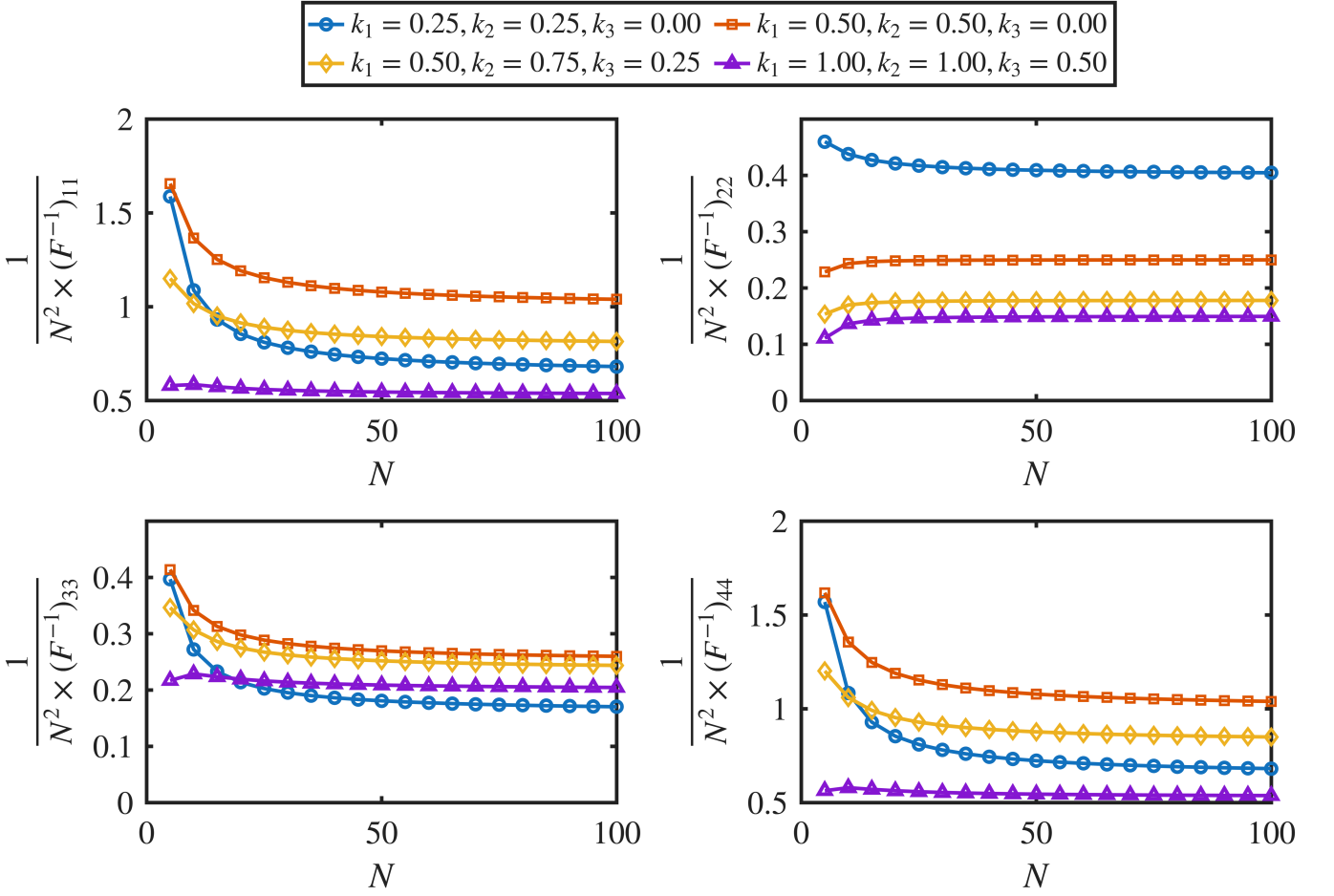


FIG. S1. Each panel shows the normalized effective Fisher information $1/(N^2 (F^{-1})_{ii})$ plotted versus the total mean photon number N for each of the four estimated parameters ϕ_0, ϕ_1, ϕ_2 , and ϕ_3 , respectively. Curves compare different LO detuning constants k_1, k_2 and balanced beam-splitter offset k_3 . A plateau of $1/(N^2 (F^{-1})_{ii})$ at large N indicates that asymptotically $(F^{-1})_{ii} \propto 1/N^2$, i.e., a Heisenberg scaling of the marginal variance for that parameter. The vertical separation between curves reflects the prefactor of the asymptotic scaling: higher plateaus correspond to larger effective Fisher information and, therefore, higher achievable precision. Differences between panels highlight that the optimal working point need not be identical for all parameters. However the asymptotic Heisenberg scaling behavior holds for different values of k_1, k_2, k_3 .

Equation (S26) shows how the Heisenberg scaling of the total Fisher information depends on the allocation of photons between squeezing and displacement through N_s and N_c . The multiparameter Cramér–Rao bound for any unbiased estimator $\tilde{\phi}$ is given by $\text{Cov}[\tilde{\phi}] \geq F^{-1}/M$. Therefore, using Eq. (S25), the marginal variances of the four parameters $\phi_0, \phi_1, \phi_2, \phi_3$ satisfy, at leading order,

$$\Delta^2 \tilde{\phi}_0 \geq \frac{1}{M N^2} [\mathcal{F}^{-1}]_{11} + O\left(\frac{1}{N}\right), \quad (\text{S27})$$

$$\Delta^2 \tilde{\phi}_1 \geq \frac{1}{M N^2} [\mathcal{F}^{-1}]_{22} + O\left(\frac{1}{N}\right), \quad (\text{S28})$$

$$\Delta^2 \tilde{\phi}_2 \geq \frac{1}{M N^2} [\mathcal{F}^{-1}]_{33} + O\left(\frac{1}{N}\right), \quad (\text{S29})$$

$$\Delta^2 \tilde{\phi}_3 \geq \frac{1}{M N^2} [\mathcal{F}^{-1}]_{44} + O\left(\frac{1}{N}\right), \quad (\text{S30})$$

as in Eqs. (11)–(14) of the main text. Equations (S27)–(S30) make explicit that all four parameters exhibit Heisenberg scaling $\Delta^2 \tilde{\phi}_i \propto 1/N^2$, with prefactors determined by the diagonal elements of the coefficient matrix \mathcal{F}^{-1} (see FIG. S1).

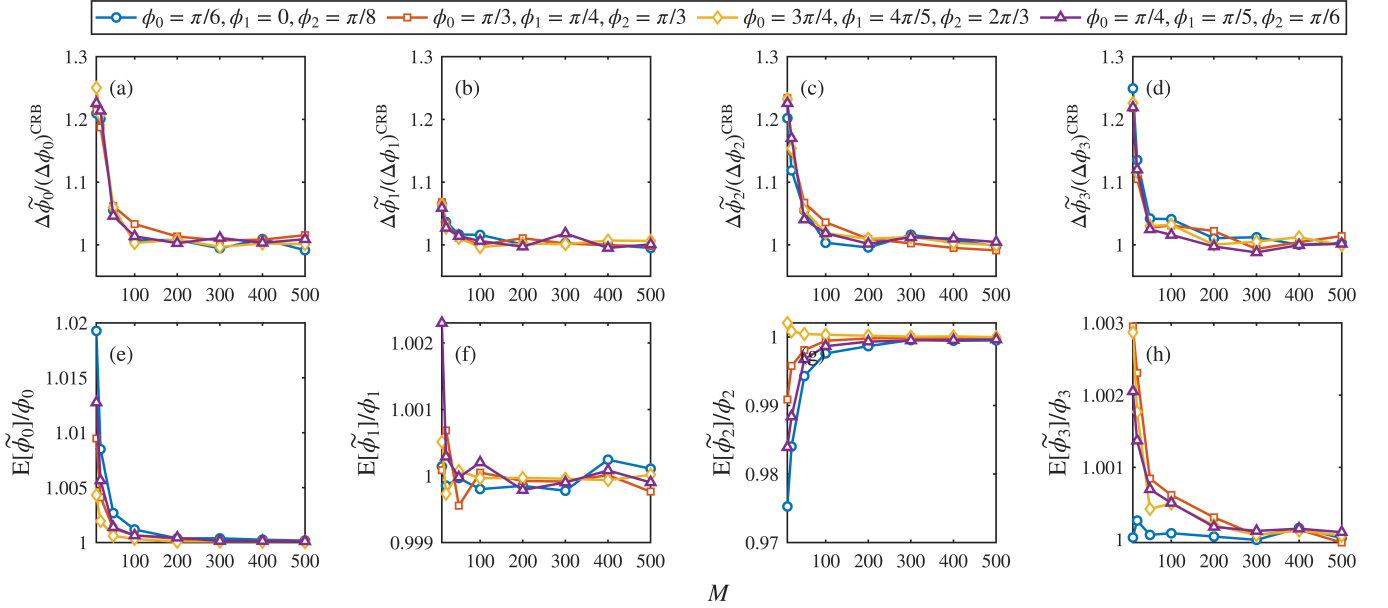


FIG. S2. Asymptotic performance of the MLEs for a total mean photon number $N = 10$ with equal resource split, $N_c = N_s = 5$. The different parameter values (ϕ_0, ϕ_1, ϕ_2) in the figure assess the robustness of the estimation to changes in the true parameter values. Top row: the normalized CRB $\Delta\tilde{\phi}_i/(\Delta\phi_i)^{\text{CRB}}$ versus the number of experimental iterations M for $i = 0, 1, 2, 3$. The convergence of all curves to unity shows that the MLE saturates the CRB in the large- M limit. Bottom row: the unbiasedness ratio $E[\tilde{\phi}_i]/\phi_i$ as a function of M for the same settings, which converges towards 1 as the estimator bias becomes negligible, typically for sample sizes of order $M \approx 100$. The beam-splitter angle is set to the balanced working point $k_3 = 0$ ($\phi_3 = \pi/4$), and the LO constants are fixed to $k_1 = k_2 = 0.5$.

Since \mathcal{F} is block diagonal, its determinant factorizes as

$$\det(\mathcal{F}) = \left(\frac{2(1-\beta)\beta}{\Lambda} D_2 \right) \det \left(\frac{\beta^2}{\Lambda^2} \begin{pmatrix} D_1 & A & B \\ A & D_3 & C \\ B & C & D_4 \end{pmatrix} \right), \quad (\text{S31})$$

since $D_2 > 0$ for all ϕ_1 and real k_1, k_2, k_3 , and for $0 < \beta < 1$, \mathcal{F} is singular iff the (ϕ_0, ϕ_2, ϕ_3) sub-block is singular. For the coefficients in Eq. (S26) one finds

$$\det \begin{pmatrix} D_1 & A & B \\ A & D_3 & C \\ B & C & D_4 \end{pmatrix} = 16384 (k_1 + k_2)^2 (k_1 k_2 - k_3^2)^2 \Lambda^3, \quad (\text{S32})$$

since $\Lambda > 0$ for real k_1, k_2, k_3 . Thus, the leading-order coefficient matrix \mathcal{F} is singular only for

$$k_1 = -k_2, \quad \text{or} \quad k_3^2 = k_1 k_2. \quad (\text{S33})$$

At these points, the leading $O(N^2)$ Fisher information loses rank, so the four-parameter model is locally unidentifiable at Heisenberg scaling, and at least one parameter combination can only be resolved from subleading terms.

III. MAXIMUM-LIKELIHOOD ESTIMATION

Here, we derive the maximum-likelihood estimators (MLEs) for the Gaussian statistics generated by two-port homodyne detection. Repeating the experiment M times yields an i.i.d. data set $\mathbf{x}_1, \dots, \mathbf{x}_M$, where each $\mathbf{x}_m = (x_{1,m}, x_{2,m})^\top$ is distributed according to $p(\mathbf{x} | \phi)$ in Eq. (4), with mean $\boldsymbol{\mu}_\phi$ and covariance Σ_ϕ . The likelihood function for ϕ is given by

$$\mathcal{L}(\phi | \mathbf{x}_1, \dots, \mathbf{x}_M) = \prod_{m=1}^M p(\mathbf{x}_m | \phi), \quad (\text{S34})$$

and the MLE $\tilde{\phi}_{\text{MLE}}$ maximizes \mathcal{L} , equivalently the log-likelihood $\ell(\phi) = \log \mathcal{L} = \sum_{m=1}^M \log p(\mathbf{x}_m | \phi)$. The estimator is obtained from the condition

$$\nabla_{\phi} \ell(\phi) \Big|_{\phi=\tilde{\phi}_{\text{MLE}}} = \mathbf{0}. \quad (\text{S35})$$

Using $\nabla_{\phi} \log(\det \Sigma_{\phi}) = \text{Tr}(\Sigma_{\phi}^{-1} \nabla_{\phi} \Sigma_{\phi})$ and rewriting the quadratic form in trace notation,

$$(\mathbf{x} - \boldsymbol{\mu}_{\phi})^{\top} \Sigma_{\phi}^{-1} (\mathbf{x} - \boldsymbol{\mu}_{\phi}) = \text{Tr} \left[\Sigma_{\phi}^{-1} (\mathbf{x} - \boldsymbol{\mu}_{\phi}) (\mathbf{x} - \boldsymbol{\mu}_{\phi})^{\top} \right],$$

one arrives at the coupled MLE equations in the compact form

$$\mathbf{0} = (\nabla_{\phi} \boldsymbol{\mu}_{\phi})^{\top} \Sigma_{\phi}^{-1} \left(\boldsymbol{\mu}_{\phi} - \frac{1}{M} \sum_{m=1}^M \mathbf{x}_m \right) + \frac{1}{2} \text{Tr} \left[(\nabla_{\phi} \Sigma_{\phi}^{-1}) \left(\Sigma_{\phi} - \frac{1}{M} \sum_{m=1}^M (\mathbf{x}_m - \boldsymbol{\mu}_{\phi}) (\mathbf{x}_m - \boldsymbol{\mu}_{\phi})^{\top} \right) \right] \Big|_{\phi=\tilde{\phi}_{\text{MLE}}}. \quad (\text{S36})$$

Equation (S36) is the standard score condition for a multivariate Gaussian model. In general, it does not admit a closed-form solution. In the main text we solve it numerically and use the resulting MLE to verify convergence of CRBs (Figs. 3 and 4 in the main text).

A useful simplification follows from the structure of the homodyne output statistics: in our scheme Σ_{ϕ} is independent of the phase ϕ_1 . Hence $\partial_{\phi_1} \Sigma_{\phi} = \mathbf{0}$, so the covariance-dependent trace term in Eq. (S36) vanishes identically in the ϕ_1 component. The MLE for ϕ_1 therefore reduces to,

$$\left[(\partial_{\phi_1} \boldsymbol{\mu}_{\phi})^{\top} \Sigma_{\phi}^{-1} \left(\boldsymbol{\mu}_{\phi} - \frac{1}{M} \sum_{m=1}^M \mathbf{x}_m \right) \right]_{\phi_1=\tilde{\phi}_{1\text{MLE}}} = 0, \quad (\text{S37})$$

where $\tilde{\boldsymbol{\mu}}_{\phi} = \frac{1}{M} \sum_{m=1}^M \mathbf{x}_m$ is the estimator of the sample mean $\boldsymbol{\mu}_{\phi}$. This makes explicit that the estimator $\tilde{\phi}_1$ is determined solely by the mean homodyne response. By contrast, the remaining parameters ϕ_0 , ϕ_2 , and ϕ_3 enter both $\boldsymbol{\mu}_{\phi}$ and Σ_{ϕ} , and their MLEs follow from the equation (S36). Figure S2 illustrates the asymptotic performance of the MLEs for different choices of the true parameter values. The results show that the estimators converge to the CRB and become effectively unbiased as the number of experimental iterations M increases, indicating that the estimation scheme remains robust under variations of the underlying parameters.